Optimizing Active and Passive Magnetic Shields in Induction Heating by a Genetic Algorithm

Peter L. Sergeant, Luc R. Dupré, *Member, IEEE*, Marc De Wulf, and Jan A. A. Melkebeek, *Senior Member, IEEE*

***Abstract*—This paper presents a method for designing optimal passive and active shields for axisymmetric induction heaters. Such shields are needed to protect human operators and external electronic equipment from stray magnetic fields. The method uses a genetic algorithm (GA) to minimize an objective function. This function reduces the magnetic field in the target area, the power dissipation in the active and passive shields, and the influence of the shields on the heating process. The GA returns the position and height of the passive shield, the optimal current for the active shield, and the number of turns of all coils. The paper describes two optimization modes: 1) optimization of only the active shield with fixed passive shield and 2) global optimization of both active and passive shields. Several passive shields are studied: electrically conductive shields and both electrically and magnetically conductive shields. The field reduction depends on the optimization mode and the passive shield properties, but always exceeds 25 dB for combined active and passive shields. Finally, the paper compares the results of the simulations to experimental measurements.**

***Index Terms*—Active shield, finite elements, genetic algorithm (GA), heating, induction, magnetic field, passive shield.**

I. Introduction

INDUCTION heater equipment is exploited for thermal treatment of a metallic specimen. This thermal treatment is obtained by huge eddy currents induced in the conductive specimen. The eddy currents result from the time-dependent magnetic field, which is generated by the excitation coil. The excitation coil also creates a magnetic field in the surrounding region. This gives rise to magnetic field levels ranging from several hundreds of μT up to some mT at a distance from the source in the range 0.1–1 m for induction heaters considered in [1] and for the layout presented in this paper (see $B_{\max}$ in Table III: $B_{\max}$ is the maximal induction in the target area. This area is at 0.3 m distance from the excitation coil, resulting in lower inductions than at 0.1 m). The operator of the equipment as well as electronic devices may be exposed to magnetic fields that are significantly higher than the reference levels in Table I indicated by the International Commission on Non-Ionizing Radiation Protection (ICNIRP) [2]. Thus, the magnetic field should be mitigated using three techniques:

- reconsideration of the induction heater design;
- passive shielding, using suitable materials to limit electromagnetic losses within the shield [3];
- active shields: proper currents in a number of compensation coils generate counter fields opposite to the main one to be reduced. Fig. 1 illustrates the principle.

TABLE I
ICNIRP Reference Levels [2] for Occupational and Public Exposure to Time-Varying Magnetic Fields (Unperturbed RMS Values) in the Relevant Range 25 Hz–10 MHz

Frequency range	Occupational B-field [μT]	Frequency range	Public B-field [μT]
0.025-0.82 kHz	25/f	0.025-0.8 kHz	5/f
0.82-65 kHz	30.7	0.8-3 kHz	6.25
0.065-1 MHz	2.0/f	3-150 kHz	6.25
1-10 MHz	2.0/f	0.15-1 MHz	0.92/f
		1-10 MHz	0.92/f

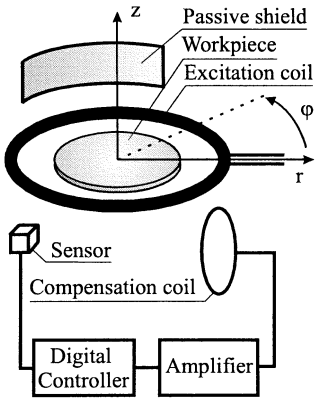

Fig. 1. Principle of active and passive shielding.

The modification of the thermal treatment of the metallic specimen by the reduction of the magnetic environmental pollution using passive and active shielding must be limited to a minimum. Moreover, the area to add shields is constrained, as the accessibility of the workpiece should be guaranteed.

The paper describes an optimization method to find the optimal active shield, possibly combined with a passive shield, that reduces the stray field of an induction heater with given geometry and material properties in a defined area. An experimental setup of an induction heater with the same geometry was built. The numerical models presented in the paper are verified by comparing the simulation results with measurements on the setup.

II. Overview of the Calculation Method

To reduce the stray field in a defined area—the target area—the optimal positions of the compensation coils and

Manuscript received March 5, 2003; revised July 21, 2003. This work was supported by GOA project 99-200/4, by the FWO project G.0309.03, and by the IUAP-project P5/34 of the Belgian government.

The authors are with the Department of Electrical Energy, Systems and Automation, Ghent University, B-9000 Ghent, Belgium (e-mail: peter.sergeant@ugent.be).

Digital Object Identifier 10.1109/TMAG.2003.819460

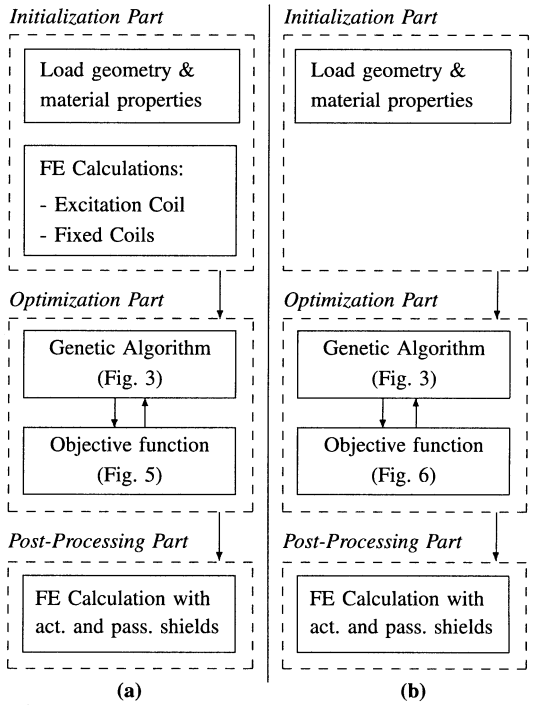

Fig. 2. Flowchart of the calculation (a) in case of active shield optimization and (b) in case of both active and passive shield optimization.

the currents in the coils must be identified from a proper inverse problem. The presented method to solve the inverse problem consists of three parts (Fig. 2): an initialization part, an optimization part—a genetic algorithm (GA) that minimizes an objective function, and a post-processing part.

The execution of the initialization and optimization part depends on the desired optimization mode:

- only active shield optimization, possibly with fixed passive shields, explained in Section II-A and Fig. 2(a);
- global optimization of both active and passive shield, explained in Section II-B and Fig. 2(b).

A. Active Shield Optimization With Fixed Passive Shield

The initialization part in Fig. 2(a) first loads the geometry and material properties of the induction heater, the geometry of the target area, and the geometrical constraints on the active and passive shields. The active shield contains N coils. Each coil has t_k turns and is positioned in (r_k, z_k) with $k = 1, 2, \ldots, N$. After the loading of the induction heater properties, a first finite-element (FE) calculation finds the stray field of the induction heater, possibly with fixed passive shields. In this calculation, only the excitation coil carries current. Next, other FE calculations are executed if not all compensation coils need an optimization of their position: for each compensation coil with fixed r and z positions, an FE calculation determines the magnetic field distribution of that coil for 1 A current in only that coil, with workpiece and passive shield present. The calculated field distributions in the target area are saved in a database for later use by the objective function.

The optimization part runs a GA, which searches the optimal positions and number of turns of the active shield coils, and the optimal compensation current (for the coils in series). The GA optimizes the positions of the coils by iteratively evaluating an objective function and trying to minimize it [4]. During each function evaluation, the compensation coil positions are fixed and the currents in the coils are optimized by the least squares method. The method minimizes the average of the B-field norms in about 500 points, defined in the target area by a proper chosen grid. Section IV explains in detail how the FE calculations in the objective function are used to find an objective value for given compensation coil positions.

Finally, in the post-processing part, an FE calculation with complete modeling of all shields is executed with high accuracy, providing full access to all electromagnetic variables in the whole domain (not only in the target area) for post-processing purpose.

B. Global Optimization of Active and Passive Shield

Once the geometry and material properties of the induction heater are loaded, the initialization part is finished [Fig. 2(b)], as no FE calculations for the excitation coil and the fixed coils field are done. If a global optimization of both passive and active shield is needed, the induction heater stray field changes every time the position, the geometry, or the material properties of the passive shield change. The magnetic field distributions have to be recalculated every time the objective function is evaluated. Thus, FE calculations in the initialization part are not useful; they are moved into the objective function, causing the evaluation time of the objective function to increase.

The optimization part runs the same GA. This time, the GA returns not only the optimal positions, number of turns, and current of the active shield coils, but also the passive shield position and height.

The post-processing part is identical to the one in Section II-A.

III. Genetic Algorithm Overview

To find the optimal compensation coil (and passive shield) positions, the global minimum of an objective function has to be searched. A gradient based optimization method [5] cannot find the global optimum [6]. Therefore, a GA is preferred. A GA is a stochastic optimization method, based on the principle of natural selection: "*the survival of the fittest individuals in a population*" [7]. The flowchart of the used algorithm, shown in Fig. 3, starts by creating an initial population, possibly consisting of a number of subpopulations. Some individuals in the population may be given by the user. The others are generated randomly, but in such a way that all individuals respect boundary and inequality constraints. Every individual $\bar{x}$ in the population contains the geometrical input arguments of the objective function: the r and/or z components of the compensation coils and possibly the position and height of the passive shield.

As GAs usually need a lot of function evaluations, some precautions have been taken to limit the number of calculations. One of these is the inequality constraints $A\bar{x} < \bar{b}$, where A is a matrix with L columns—L is the number of variables in each individual $\bar{x}$—and with one row for every constraint. $\bar{b}$ is a vector with the same number of rows. The inequality constraints are

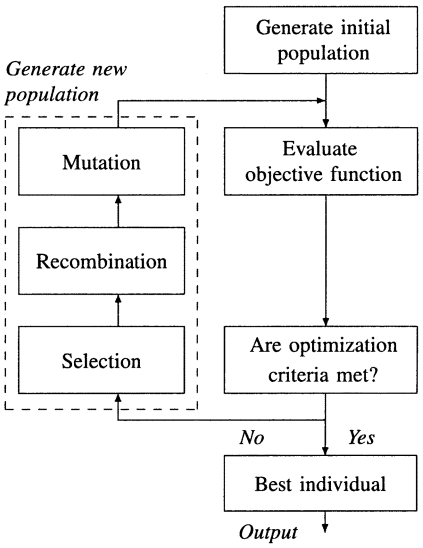

Fig. 3. Flowchart of a GA for one population.

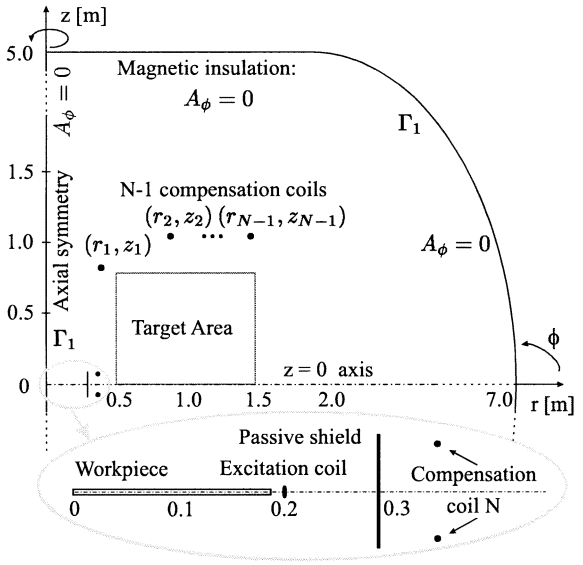

Fig. 4. Finite-element layout, scales in meter (FEM: magnetic vector potential $\overline{A} = A_\phi \overline{1_\phi}$).

applied to the N compensation coils above the symmetry plane $z = 0$ and to the N coils beneath the plane: compensation coil $k+1$ must have a higher diameter than compensation coil k ($k = 1, \ldots, N-2$, with N the number of compensation coils) and compensation coil N must have a higher diameter than the passive shield. For example: for an optimization with fixed passive shield and N not fixed compensation coils, the inequality constraints $A\bar{x} < \bar{b}$ become

$$\overbrace{\begin{matrix} r_1 & z_1 & r_2 & z_2 & r_3 & \cdots & z_N \end{matrix}}^{L \text{ columns}}$$

$$\begin{bmatrix} 1 & 0 & -1 & 0 & 0 & \cdots & 0 \\ 0 & 0 & 1 & 0 & -1 & \cdots & 0 \\ \vdots & \vdots & \vdots & \vdots & \vdots & \ddots & \vdots \\ 0 & 0 & 0 & 0 & 0 & \cdots & -1 \end{bmatrix} \begin{bmatrix} x_1 \\ x_2 \\ \vdots \\ x_N \end{bmatrix} \leq \begin{bmatrix} -d \\ -d \\ \vdots \\ -d \end{bmatrix}$$

with d the minimal radial distance between two adjacent coils. Next to the $2 \times (N-1)$ first compensation coils, of which $N-1$ are placed above the operator's head and $N-1$ beneath his feet, an Nth compensation coil and its symmetrical coil are situated close to the passive shield and the symmetry line $z = 0$ (Fig. 4). The $N-1$ inequality constraints produce $N-1$ rows in A and in $\bar{b}$. The constraints reduce the range of the variables in the GA and speed up its convergence. They do not influence the area in which the coils can be placed as still each coil can be placed at any position between the upper and lower boundary. Thus, all initially generated individuals respect not only the upper and lower boundaries, but also the inequality constraints. These constraints are realized by back-substitution:[1] $[L - \text{rank}(A)]$ variables are randomly chosen within their boundaries. The remaining rank(A) variables are to be found using the rank(A) inequality constraints. At least one of these constraints contains only one unknown variable. The boundaries of this variable are adjusted such that this variable can be chosen randomly between its (adjusted) boundaries, without violating the constraints. Once this variable is chosen, there is a new constraint that contains only one unknown variable. The procedure is repeated until all variables are chosen.

After each generation of new individuals, the new objective values are calculated and the individuals are ranked using their objective values. A new generation of individuals has to be created as illustrated in Fig. 3.

- *Selection:* The individuals obtain a fitness that represents their reproduction probability. The best individuals in every subpopulation are selected. The selection method is universal stochastic sampling [8].
- *Recombination:* The next step is recombination (crossover) between the fittest individuals: some of the variables of two individuals are exchanged [9]. Recombination is only executed if the inequality constraints are respected.
- *Mutation:* All variables in an individual obtained after recombination have a small chance on mutation [10]. The range in which a variable can mutate is chosen such that inequality and boundary constraints are not violated and that small mutation steps are more likely than large changes of the value of a variable.
- *Reinsertion:* If in the used GA the number of children is smaller than the number of parents (due to selection), a proper number of parents is reinserted into the new generation to obtain the same size of the population.
- *Migration:* If the population consists of more than one subpopulation, all subpopulations will live isolated for a few generations. After a few generations, 20% of the individuals—randomly selected—migrate from one subpopulation to another to increase the diversity.

The GA terminates if one of three criteria is fulfilled.

[1]Back-substitution is used for the solving of matrix equations $A\bar{x} = \bar{b}$. A is made upper-triangular by QR-factorization and then solved by back-substitution. It can be used for choosing variables in matrix inequalities if the matrix is upper or lower triangular. However, if the variables have to respect boundary constraints as well, a solution is not guaranteed: some variables may be chosen such that the remaining ones cannot be chosen any more without violating the boundaries or the constraints. If in this calculation no range is left within which to choose a variable, the previously chosen variables are modified such that again a range is available for the last variable.

- The maximum number of generations is reached.
- The mean of the objective values does not change any more within a certain tolerance.
- The time limit is exceeded.

IV. Objective Function Overview

The objective function calculates the "cost" of an active and a passive shield with the compensation coil positions (and the passive shield position and height) as inputs. Similar to Section II, two optimization modes are considered.

A. Active Shield Optimization With Fixed Passive Shield

The flowchart of the objective function is shown in Fig. 5. To optimize the compensation current, the function needs the field distributions of the excitation coil and each of the N compensation coils. Therefore, a finite-element model for every coil is used, as explained in Section V. However, the field of the excitation coil and the fields of all fixed compensation coils are not calculated any more, as they have already been calculated in the initialization part [Fig. 2(a)]. The field distributions of the non-fixed coils are calculated, but only if they are not found in the database. The new field distribution is saved. If in the future a coil has the same coordinates, the required calculation will be replaced by a reading from memory. Saving field distributions is only useful if the number of possible coil positions is limited. Therefore, the coils are given discrete positions (resolution, for example, 5 mm). Next to the inequality constraints, the discrete coil positions are a second precaution to reduce the calculation time: the more function evaluations the GA performs, the more probable it is that a field distribution can be read from file instead of calculated. The evaluation time decreases significantly, as FE calculations are the most time-consuming part in the evaluation of the objective function. Once all necessary field distributions gathered, the objective function searches the optimal compensation current as explained in Section IV-B.

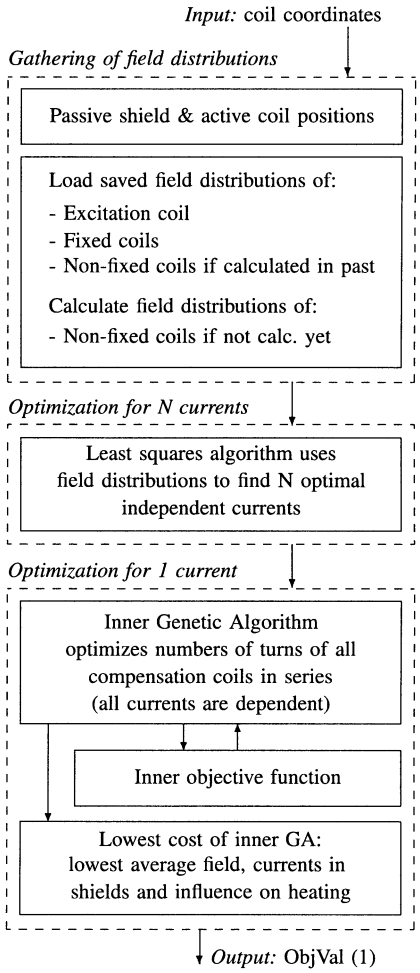

Fig. 5. Flowchart of objective function in case of active shield optimization.

B. Global Optimization of Active and Passive Shield

As the field distributions of the excitation coil and of fixed coils depend on the passive shield geometry, they are not saved during the initialization part in Fig. 2. These field distributions have to be calculated for every evaluation of the objective function. The flowchart of Fig. 5 is still valid, except the first part (the gathering of the field distributions) that is replaced, as shown in Fig. 6. In this optimization mode, only one field distribution is saved for every discrete position and height of the passive shield: the stray field of the induction heater generated by the excitation coil only. The fields of all compensation coils have to be recalculated in every function evaluation, as they depend on four parameters (r and z coordinate of the coil, position, and height of the passive shield).

C. Finding the Value of the Objective Function

The finding of the objective value is the same for both optimization modes; see "Optimization for N currents" and "Optimization for 1 current" in Fig. 5 and in Fig. 6. A least-squares algorithm finds the best N independent currents in all N coils using the calculated field distributions (Section VI). In the experimental setup, however, all coils are in series in order to keep the installation cost of the supplies for the active shielding low. Based on the found N independent currents, the best number of turns and best current are searched, giving the lowest cost with only one independent compensation current. To find this current, a second least-squares algorithm is used; the optimal number of turns are found by a second GA, nested within the objective function of the main GA.[2] The initial population of this algorithm is based on the optimal N independent currents. The objective value returned to the main GA is the best objective value of the inner GA. This main objective value

$$\mathrm{ObjVal} = w_1 \int_{\mathrm{TA}} \frac{|B|}{S_{\mathrm{TA}}} dr\, dz + w_2 \sum_{i=1}^{N} |t_i| I_{\mathrm{com}}^2 + w_3 W_{\mathrm{Sh}} + w_4 (W_{\mathrm{Wp,noSh}} - W_{\mathrm{Wp,Sh}}) \quad (1)$$

contains four terms with corresponding weighting factors w_1, w_2, w_3, and w_4. The first is the average norm of the magnetic induction in the target area: the integral of $|B|$ divided by the surface of the target area S_{TA}. The second and third take

[2]As this inner GA optimization is a random process; the main objective function returns other objective values if it is called several times with the same input arguments. The main GA, however, seems robust enough to optimize the stochastic objective function.

into account the dissipation in the active and passive shield: the second term penalizes the compensation current I_{com} and the number of turns t_i, and the third symbolizes the heat dissipation W_{Sh} in the passive shield. Finally, the fourth term describes the influence of the shields on the heating process. $W_{\mathrm{Wp,noSh}}$ is the induced power in the workpiece without passive or active shields. $W_{\mathrm{Wp,Sh}}$—the energy dissipation in the workpiece with shields present—decreases when adding a passive shield, especially when a passive shield is close to the excitation coil. The third and fourth term are necessary to inhibit the GA to choose a large passive shield very close to the excitation coil.

For the inner GA, four termination criteria are set: the three criteria that are used for the main GA and an additional one—the difference to the optimum. The objective values of the inner GA are compared to the minimal average magnetic field in the target area, obtained with N independent currents. This is the lowest possible objective value: the average field in the target area is the lowest, and no dissipations are taken into account $(w_2 = w_3 = w_4 = 0)$. The inner GA algorithm terminates if an objective value is close enough to this lowest possible value.

V. Numerical Model for the Environment of the Induction Heater

An FE model for the passive and active shielding of the magnetic stray field of induction heaters is developed [11]. The linear model is axisymmetric, quasi-static, and time-harmonic. The domain Ω is defined by the induction heater, the passive shield, the compensation coils, and the air surrounding the induction heater. Fig. 4 illustrates the geometry. Due to symmetry with respect to $z = 0$, only the properties in the space $z > 0$ are shown. The modeled induction heater consists of a one-turn excitation coil of 20.27-cm radius and an aluminum workpiece to be treated thermally with a radius of 191 mm. Other properties can be found in Table II. This layout was chosen as it corresponds to the experimental setup of an induction heater for the thermal treatment of wheels. The numerical model can easily be changed to another geometry of the workpiece (instead of a disk, e.g., a wire, torus, cone, etc.) and of the excitation coil (instead of a coil with one winding, e.g., a coil with several distributed windings below, above, and next to the workpiece, other coil sections, etc.) on condition that the geometry is axisymmetric.[3] A 1-m-long and 0.8-m-high rectangle symbolizes the target area where the operator is working and where the average magnetic induction B should be minimized. Above the target area, a number of compensation coils can be found in Fig. 4. These coils should minimize the magnetic induction in the target area. However, very high compensation currents are needed to reduce B in the lower left corner of the target area: the maximum value of B will occur in this corner—the region closest to the excitation coil—and the active compensation coils are further away of this area than the excitation coil. Thus, one extra compensation coil and a small passive shield have been added, at radius between 22 and 48 cm to reduce the field in the lower left corner of the target area. The passive shield and compensation coil N increase the efficiency of the other $N - 1$ compensation coils. In the numerical field calculation, the known current density in the compensation coils is denoted by $\bar{J}_e = J_e(r,z)\bar{1}_\phi$. In the domain Ω, the magnetic induction is written as $\bar{B} = \bar{\nabla} \times \bar{A}$, with the vector potential $\bar{A} = A_\phi(r,z)\bar{1}_\phi$. It is well known from Maxwell equations that $A_\phi(r,z)$ obeys a second-order boundary value problem in Ω, i.e.,

$$\frac{\partial}{\partial r}\left[\frac{1}{r\mu}\frac{\partial}{\partial r}(rA_\phi)\right] + \frac{\partial}{\partial z}\left[\frac{1}{r\mu}\frac{\partial}{\partial z}(rA_\phi)\right] - i\sigma\omega A_\phi = -J_e \quad (2)$$

together with the boundary condition (BC); see Fig. 4

$$A_\phi = 0 \text{ on } \Gamma_1. \quad (3)$$

Here, μ and σ are the permeability and the electric conductivity of the material present in Ω. $f = \omega/2\tau$ is the frequency of the source term J_e. The BC on Γ_1 describes magnetic isolation. On

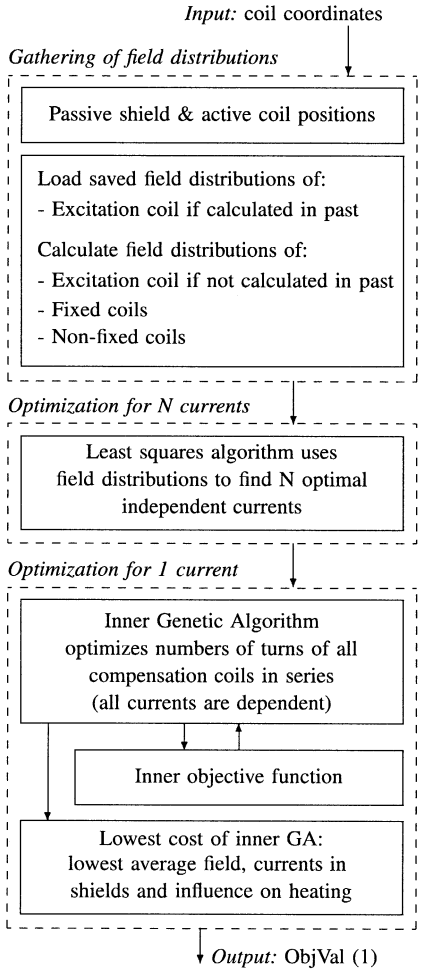

Fig. 6. Flowchart of objective function in case of global optimization of active and passive shield.

[3]For nonaxisymmetric induction heaters, a three-dimensional (3-D) model can be designed that can replace the two-dimensional (2-D) calculations in the objective function. With small changes to the objective function concerning, e.g., the geometrical constraints on the 3-D compensation coils and the storage of the 3-D field distributions, the main GA should work properly for generalized multiwinding induction heaters. However, due to the high evaluation time of a 3-D FE model combined with a possibly high number of optimization variables (more variables for one coil), the optimization requires one or more very performant computers.

TABLE II
GEOMETRICAL AND ELECTROMAGNETIC PROPERTIES OF THE EXCITATION COIL, THE WORKPIECE, AND THE TWO STUDIED PASSIVE SHIELDS. IN THE EXCITATION COIL, 4 kA CURRENT IS FORCED; $\sigma = 0$ MEANS THAT NO SKIN EFFECT IS TAKEN INTO ACCOUNT. DIMENSION OF RADIUS AND THICKNESS ARE ALONG THE R AXIS; DIMENSION OF HEIGHT IS ALONG THE Z AXIS

Property	Outer Radius [m]	Thickness [mm]	Height [mm]	σ [$(\Omega m)^{-1}$]	μ $\times\mu_0$
Excit. coil	0.2027	1.50	16.0	0	1
Workpiece	0.1910	-	10.0	$3.7 \cdot 10^7$	1
Steel pas. sh.	0.3065	0.65	190	$5.9 \cdot 10^6$	372
Copper pas. sh.	0.3050	0.50	190	$5.2 \cdot 10^7$	1

the symmetry plane $z = 0$, a boundary condition forcing the flux lines to be normal to the symmetry plane could be used

$$\left(\frac{1}{r}\frac{\partial}{\partial r}(rA_\phi)n_r + \frac{1}{r}\frac{\partial}{\partial z}(rA_\phi)n_z\right) = 0 \text{ on } z = 0. \quad (4)$$

With this boundary condition, the size of the domain Ω can be reduced to 1/2, as well as the number of elements in the FE mesh. However, to be compatible with the experimental setup that is built on a floor containing conductive materials, two small conductive regions were to be added to the FE models at large distance from the induction heater. Measurements were used to determine the material properties of these two regions by trial and error. The domains make the model unsymmetrical with respect to the $z = 0$ axis. Consequently, we considered the whole region for the FE computations. For the passive shield, two materials are used in the calculations. Their properties μ_p and σ_p are experimentally determined and can be found in Table II.

VI. THE LEAST-SQUARES METHOD

A. N Independent Optimal Currents

In the model, N compensation coils are considered. In a time-harmonic calculation, $\bar{B} = B_r\bar{1}_r + B_z\bar{1}_z$ consists in each point of two complex components $B_r = B_{r,r} + iB_{r,i}$ and $B_z = B_{z,r} + iB_{z,i}$. Similarly, the current $I_k\bar{1}_\phi$ in compensation coil k has a real and imaginary component: $I_k = I_{r,k} + iI_{i,k}$. When the compensation coil k carries $I_k = (1 + 0i)$ A current, with zero current in all other coils and with the passive shield and workpiece present, the r and z components of $\bar{B}$ are denoted by $b_{r,r,k}$, $b_{r,i,k}$, $b_{z,r,k}$, and $b_{z,i,k}$. The total induction, generated by the excitation coil and N compensation coils, is

$$\begin{aligned}
B_{r,r} &= B_{r,r,e} + \sum_{k=1}^{N}(b_{r,r,k}I_{r,k} - b_{r,i,k}I_{i,k}) \\
B_{r,i} &= B_{r,i,e} + \sum_{k=1}^{N}(b_{r,i,k}I_{r,k} + b_{r,r,k}I_{i,k}) \\
B_{z,r} &= B_{z,r,e} + \sum_{k=1}^{N}(b_{z,r,k}I_{r,k} - b_{z,i,k}I_{i,k}) \\
B_{z,i} &= B_{z,i,e} + \sum_{k=1}^{N}(b_{z,i,k}I_{r,k} + b_{z,r,k}I_{i,k}) \quad (5)
\end{aligned}$$

with $B_{r,r,e}$, $B_{r,i,e}$, $B_{z,r,e}$, and $B_{z,i,e}$ the real and imaginary r and z contribution of the excitation current in the presence of the passive shield and the workpiece. The norm of the induction B is the square root of

$$B^2 = B_{r,r}^2 + B_{r,i}^2 + B_{z,r}^2 + B_{z,i}^2. \quad (6)$$

The matrix A is constructed from the partial derivatives of B^2 to the currents $I_{r,k}$ and $I_{i,k}$

$$\left[\begin{array}{ccc|ccc}
\frac{\partial B^2}{\partial I_{r,1}^2} & \frac{\partial B^2}{\partial I_{r,1}\partial I_{r,2}} \cdots & \frac{\partial B^2}{\partial I_{r,1}\partial I_{r,N}} & \frac{\partial B^2}{\partial I_{r,1}\partial I_{i,1}} \cdots & \frac{\partial B^2}{\partial I_{r,1}\partial I_{i,N}} \\
\frac{\partial B^2}{\partial I_{r,2}\partial I_{r,1}} & \frac{\partial B^2}{\partial I_{r,2}^2} \cdots & \frac{\partial B^2}{\partial I_{r,2}\partial I_{r,N}} & \frac{\partial B^2}{\partial I_{r,2}\partial I_{i,1}} \cdots & \frac{\partial B^2}{\partial I_{r,2}\partial I_{i,N}} \\
\vdots & \vdots \ddots & \vdots & \vdots \ddots & \vdots \\
\frac{\partial B^2}{\partial I_{r,N}\partial I_{r,1}} & \frac{\partial B^2}{\partial I_{r,N}\partial I_{r,2}} \cdots & \frac{\partial B^2}{\partial I_{r,N}^2} & \frac{\partial B^2}{\partial I_{r,N}\partial I_{i,1}} \cdots & \frac{\partial B^2}{\partial I_{r,N}\partial I_{i,N}} \\
\hline
\frac{\partial B^2}{\partial I_{i,1}\partial I_{r,1}} & \frac{\partial B^2}{\partial I_{i,1}\partial I_{r,2}} \cdots & \frac{\partial B^2}{\partial I_{i,1}\partial I_{r,N}} & \frac{\partial B^2}{\partial I_{i,1}^2} \cdots & \frac{\partial B^2}{\partial I_{i,1}\partial I_{i,N}} \\
\frac{\partial B^2}{\partial I_{i,2}\partial I_{r,1}} & \frac{\partial B^2}{\partial I_{i,2}\partial I_{r,2}} \cdots & \frac{\partial B^2}{\partial I_{i,2}\partial I_{r,N}} & \frac{\partial B^2}{\partial I_{i,2}\partial I_{i,1}} \cdots & \frac{\partial B^2}{\partial I_{i,2}\partial I_{i,N}} \\
\vdots & \vdots \ddots & \vdots & \vdots \ddots & \vdots \\
\frac{\partial B^2}{\partial I_{i,N}\partial I_{r,1}} & \frac{\partial B^2}{\partial I_{i,N}\partial I_{r,2}} \cdots & \frac{\partial B^2}{\partial I_{i,N}\partial I_{r,N}} & \frac{\partial B^2}{\partial I_{i,N}\partial I_{i,1}} \cdots & \frac{\partial B^2}{\partial I_{i,N}^2}
\end{array}\right]$$

while

$$C = \left[\begin{array}{ccc|ccc}
\frac{\partial B^2}{\partial I_{r,1}} & \frac{\partial B^2}{\partial I_{r,2}} & \cdots & \frac{\partial B^2}{\partial I_{r,N}} & \frac{\partial B^2}{\partial I_{i,1}} & \cdots & \frac{\partial B^2}{\partial I_{i,N}}
\end{array}\right]^T$$

with

$$\begin{aligned}
I_{r,1} &= I_{r,2} = \ldots = I_{r,N} = 0 \\
I_{i,1} &= I_{i,2} = \ldots = I_{i,N} = 0.
\end{aligned}$$

In the target area, a proper grid is chosen. In every grid point, the matrices A and C are calculated. Finally, all matrices are summed over the P points in the grid and the following linear set of equations is solved:

$$\left(\sum_{k=1}^{P} A\right) I = -\sum_{k=1}^{P} C \quad (7)$$

wherein $I = [I_{r,1}, \ldots, I_{r,N} | I_{i,1}, \ldots, I_{i,N}]^T$. I is the vector with the optimal currents in the N compensation coils, for fixed coil positions and excitation current.

B. N Dependent Optimal Currents

The least-squares problem with N variables is rewritten for two variables—real and imaginary part of only one compensation current—taking into account the number of turns of each coil. Equation (7) is solved, but matrices A and C change to $A' = TAT^T$ and $C' = TC$, with

$$T = \underbrace{\left[\begin{array}{cccc|cccc}
t_1 & t_2 & \cdots & t_N & 0 & 0 & \cdots & 0 \\
0 & 0 & \cdots & 0 & t_1 & t_2 & \cdots & t_N
\end{array}\right]}_{2N \text{ columns.}} \quad (8)$$

The inner GA optimizes the number of turns by using the described least-squares method. The least-squares method calculates the best current in an active shield with fixed coil positions and fixed number of turns. The initial population of the inner GA is based on the optimized N currents for the case of the N independent currents. A good initial population reduces the computation time to find the optimum. The number of turns, providing the smallest value for (1), are kept and passed to the main objective function. A positive number of turns for a coil

means that the orientation of the winding is the same as the orientation of the excitation coil. For practical reasons, the number of turns should be chosen rather low: the limit is ten.

VII. Simulation Results

For the excitation current, a sinusoidal excitation current as high as 4 kA at 1 kHz is used in the simulation, which is necessary to heat the workpiece quickly.[4] Five situations of shielding are considered:

- the unshielded induction heater;
- shielding with only passive shields;
- shielding with only active shields;
- shielding with a fixed passive shield and optimized active shield;
- shielding with globally optimized passive and active shield.

A. No Active or Passive Shield

Without any passive or active shield, the magnetic induction norm and its direction in the relevant part of the domain Ω are shown in Fig. 7. The average value of B in the target area is 28.9 μT, as shown in Table III. The maximum value of 196.5 μT is found in the lower left corner of the target area.

The energy dissipation in the workpiece $W_{\rm wp}$ is determined by integrating the energy dissipation of the induced eddy currents over the volume of the disk

$$W_{\rm wp} = 2\pi \int_S \frac{J^2}{\sigma} r \, dr \, dz, \text{ with } J = -i\sigma\omega A_\phi \qquad (9)$$

With 4-kA ampere current (frequency 1 kHz) in the one turn-excitation coil, $W_{\rm wp}$ is 1.97 kW, mainly situated in the region $0.187 \text{ m} < r < 0.191$ m. Fig. 8 shows the dissipation in the workpiece for several frequencies. When adding shields, the change of $W_{\rm wp}$ should be limited to keep the heating process unaltered.

B. Passive Shield

The field reduction obtained by adding a passive shield strongly depends on the position, the height, and the electromagnetic properties of the shield. Table III shows the average induction norm in the target area and the induced heating in the workpiece and in the passive shield for both the steel and the copper shield with properties in Table II. Copper seems to cause lower B levels in the target area and lower energy dissipation in the passive shield than steel, but has more influence on the heating process. Indeed, Fig. 9 shows for both steel and copper shields the average induction in the target area for a 19-cm-high shield at several positions between the excitation coil (at 0.202 m) and the left edge of the target area (at 0.5 m). It is obvious that this average induction in the target area decreases as the passive shield is closer to the excitation coil. A copper shield seems to reduce the average field more efficiently than a steel one, regardless of its position. Apart from the average induction, the condition that the heating process must not be changed by the shields has to be taken into account. Fig. 9 also shows the relative power induced in the workpiece, compared to the power in the unshielded case. Unfortunately, the best shields have the strongest impact on the heating process. When designing induction heater shields, the maximal power decrease in the workpiece caused by the adding of the shields should be defined. The same conclusions can be taken when varying the height of the shield at fixed position of 0.3 m (Fig. 10).

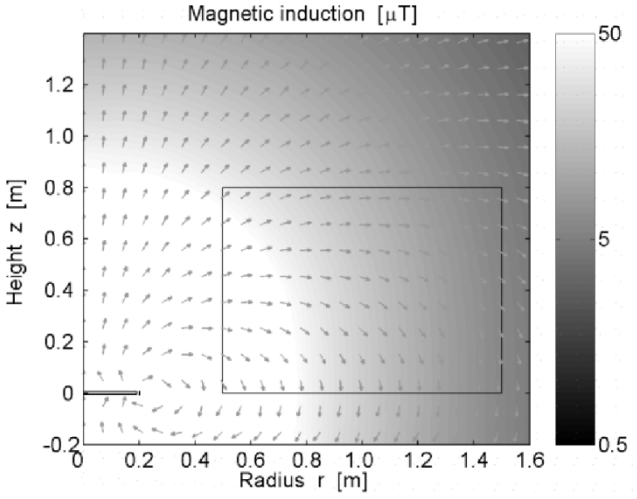

Fig. 7. Magnetic induction in case no shields are implemented.

C. Optimized Active Shield

The active shield consists of nine compensation coils. Nine coils require 18 variables to determine their r and z coordinates, but not all of them are optimized. The GA used for active shield optimization considers 11 variables. Indeed, only three coils have both r- and z-component optimized, which results in six variables. Five coils have a fixed height (only the five r components are optimized). The ninth coil has fixed coordinates to limit the number of variables: it is at a noncritical position, far from the excitation coil. All coil positions are constrained as not all coil positions are convenient, due to the needed accessibility of the workpiece.

- One compensation coil has a fixed position at $(r, z) = (1.5 \text{ m}, 1.15 \text{ m})$.
- The r position of all other coils is in the range 0.210–1.45 m (radius).
- The radius of coil k is at least 40 mm more than the radius of coil $k-1$, for coils 2–8.
- Coils 3 to 8 have a fixed z position, at 1.15 m above the symmetry plane $z = 0$.
- Coil 9 is rather close to the excitation coil: $0.33 \text{ m} < r < 0.48$ m and $0.01 \text{ m} < z < 0.15$ m.

The population in the main GA consists of 150 individuals, separated into five subpopulations. The GA calculated 12 generations on a 1-GHz personal computer, consuming eight days of CPU time. By restricting the number of possible coil positions through rather tight boundaries and inequality constraints on the

[4]During the heating process, the temperature-dependent conductivity of the workpiece changes. However, the simulation considers the conductivity constant and, thus, calculates the optimal compensation coil positions for a certain temperature of the workpiece. This is logical as the coil positions cannot be changed during the heating process. It is the compensation current that has to be updated regularly by solving a coupled thermal-electromagnetic problem. This problem can be solved using time-stepping, but with fixed positions of the compensation coils.

TABLE III
FOR SEVERAL SHIELDING SITUATIONS WITH ACTIVE AND/OR PASSIVE STEEL (FE) OR COPPER (CU) SHIELDS: AVERAGE AND MAXIMAL B IN THE TARGET AREA, INDUCED HEATING IN THE WORKPIECE $W_{\rm wp}$ AND IN THE PASSIVE SHIELD W_p, WEIGHTING FACTORS IN (1)

Shields		Optimized values				Weighting factors			
Passive	Active	B_{avg}	B_{max}	W_{wp}	W_p	w_1	w_2	w_3	w_4
None	None	28.9 μT	196.5 μT	1.97 kW	-	10^9	0	0	0
None	Optim.	4.18 μT	141.3 μT	1.93 kW	-	10^9	3	0	0
Fe, fix	None	9.59 μT	55.1 μT	1.89 kW	267 W	10^9	0	0	0
Fe, fix	Optim.	1.59 μT	23.6 μT	1.87 kW	211 W	10^9	0.05	0	15
Fe, opt.	Optim.	2.99 μT	46.9 μT	1.89 kW	191 W	10^9	3	5	10
Cu, fix	None	4.03 μT	21.6 μT	1.78 kW	81.5 W	10^9	0	0	0
Cu, fix	Optim.	0.904 μT	15.9 μT	1.78 kW	71.9 W	10^9	0.05	0	30
Cu, opt.	Optim.	0.532 μT	9.57 μT	1.63 kW	169 W	10^9	0.05	5	30

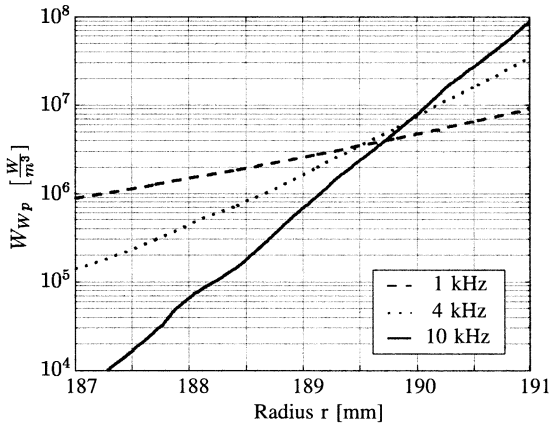

Fig. 8. Induced resistive heating in the workpiece.

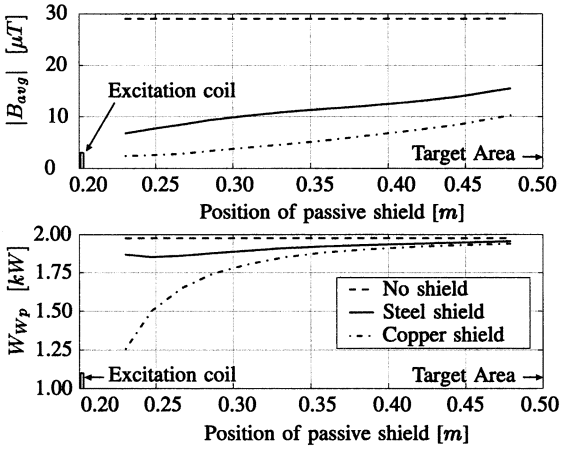

Fig. 9. Average induction in target area and induced heating in workpiece, in function of the radial position of a 19-cm-high passive shield.

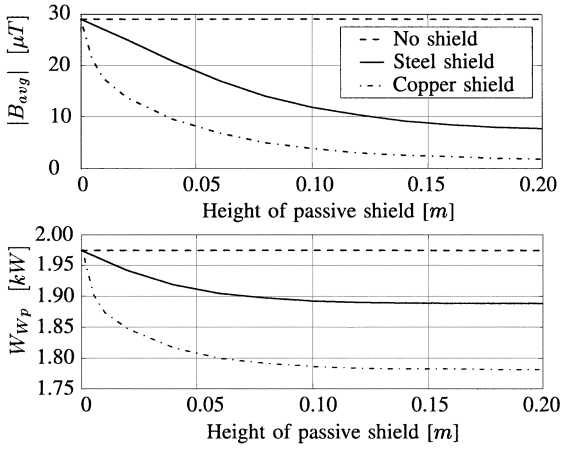

Fig. 10. Average induction in target area and induced heating in workpiece, in function of the height of a passive shield at 0.3-m radius.

variables, the GA converges faster to an optimum. The number of generations may be too low to conclude that the found coil positions realize the global optimum, but as during several generations only small changes of the best objective value occurred, we assume that the distance to the global optimum is very small.

Table III shows the results of the optimization and also the weighting factors to calculate the objective value (1) of the individuals. Only the average induction in the target area and the compensation current were taken into account: $w_1 \neq 0$ and $w_2 \neq 0$. The average value of B in the target area is 4.18 μT (Table III), a reduction by only 17 dB. The reason is the high field of 141 μT in the lower left corner of the target area. A high current is needed in this area to reduce the field. No passive shield is available, so the active shield has to generate all current itself. The compensation current amplitude is penalized by w_2 in (1), but is not limited by a boundary. A high compensation current is expected. However, the best solution for the current is only $10.54 - 1.14i$ A for $4.0 + 0i$ kA excitation current. The penalization by w_2 is partially the reason for the rather low current:[5] a higher w_2 would certainly cause a lower compensation current. The main reason is that a too high current in all coils (in series) makes effective field reduction impossible: in the majority of coils, the current is too high even with one turn. Only the number of turns can be varied, but no coil is allowed to have more than $t_{\max} = 10$ turns. This explains the choice of the turns in Table IV: coil 9—the coil close to the passive shield—has the maximum number of ten, while most of the others have zero because the compensation current is too high to achieve good field reduction, even with one turn. With a higher choice of $t_{\max}$—e.g., n times higher—probably less coils would have zero turns as the compensation current would be n times smaller. Notice that the total current in coil 9 with $nt_{\max}$ turns instead of $t_{\max}$ and $I_{\rm opt}/n$ line current remains the same. The

[5]The first term in (1) is $w_1 B_{\rm avg}/S_{\rm TA} = 10^9 \times 4.18 \times 10^{-6}\ {\rm T}/0.8\ {\rm m}^2 = 5225$, while the second term is $w_2 \sum_{i=1}^{N} |t_i| I_{\rm com}^2 = 5057$.

TABLE IV
FOR ACTIVE SHIELD OPTIMIZATION WITH SEVERAL PASSIVE SHIELDS: COMPENSATION COIL POSITIONS, OPTIMAL COMPENSATION CURRENT, AND NUMBER OF COIL TURNS

Shield	**None, opt.**			**Steel, fix**			**Steel, global opt.**			**Copper, fix**			**Copper, global opt.**		
I_{opt}	$10.54 - 1.14i$ A			$-11.95 + 9.36i$ A			$0.68 - 1.89i$ A			$-3.74 + 2.87i$ A			$0.18 - 1.43i$ A		
Coil	r_i [m]	z_i [m]	t_i	r_i [m]	z_i [m]	t_i	r_i [m]	z_i [m]	t_i	r_i [m]	z_i [m]	t_i	r_i [m]	z_i [m]	t_i
1	0.430	0.790	3	0.225	0.945	6	0.235	0.525	2	0.225	0.500	4	0.245	1.010	9
2	0.645	0.905	1	0.280	0.980	−4	0.305	1.140	1	0.400	0.995	−1	0.385	0.900	1
3	0.690	1.150	0	0.635	1.150	1	0.355	1.150	1	0.580	1.150	−1	0.795	1.150	−1
4	0.735	1.150	0	0.665	1.150	0	0.505	1.150	6	0.915	1.150	4	0.885	1.150	1
5	1.025	1.150	0	0.695	1.150	−2	0.655	1.150	1	1.090	1.150	−10	1.075	1.150	−2
6	1.080	1.150	0	0.730	1.150	1	0.845	1.150	0	1.150	1.150	8	1.265	1.150	4
7	1.445	1.150	0	1.220	1.150	0	1.435	1.150	0	1.400	1.150	−2	1.450	1.150	−5
8	1.500	1.150	1	1.500	1.150	0	1.500	1.150	1	1.500	1.150	1	1.500	1.150	3
9	0.440	0.105	−10	0.330	0.150	9	0.445	0.145	-10	0.360	0.150	10	0.400	0.110	−10

optimal value of $t_{\max}$ depends on the voltage and current range of the power supply for the active shield.

D. Passive Shield and Optimized Active Shield

A passive shield with 190-mm height and 0.3-m radius is added to the model. With the steel passive shield, the model is not linear anymore in the excitation and compensation currents, because the permeability μ_p of the passive shield depends slightly on the magnetic field H. However, as the amplitude of the excitation current is constant and the small compensation currents hardly influence the magnetic field around the passive shield, we can linearize the model by assuming μ_p equal to a constant shown in Table II.

The population consists again of 150 individuals, separated into five subpopulations. On the limit of eight days CPU time, the GA calculated 12 generations. By restricting the number of possible coil positions through rather tight boundaries and inequality constraints on the variables, the necessary number of generations may be rather low. Every new generation, the best objective value found in the generation decreased until generation 8. As during the last four generations hardly better individuals were found, we can assume that the global optimum is approximated well.

With a passive shield in steel, we obtain an average induction of 1.59 μT with only six coils, as three of the nine coils have zero turns. For an excitation current of $4.0 + 0i$ kA, the compensation current is $-11.95+9.36i$ A, less than 0.5% of the excitation current. The total number of turns is 2×23. The coil positions can be found in Table IV. This global optimization of the active shield by the GA is better than a local optimization with a gradient based algorithm [6], where the average induction was 2.18 μT. The induced resistive heating in the workpiece $W_{\rm wp}$ is 1.87 kW, which means a slight decrease, compared to 1.97 kW in the unshielded case. There is a significant energy dissipation in the passive shield, which equals about 11% of the heating in the workpiece.

With a copper passive shield, the average B in the target area is only 0.90 μT, but the reader will notice that the reduction of 30 dB is mainly due to the passive shield itself (17 dB); the reduction by the active shield is quite small (13 dB) compared to its reduction if a steel passive shield is used. The large eddy currents in the copper shield do not have the same phase as the induction heater stray field. Thus, the required phase of the compensation current in the area short to the copper sheet differs from the required phase at a larger distance. As only one compensation current is provided to all coils in series, only one phase can be chosen and the field cannot be reduced effectively in the whole target area. The steel sheet has a higher resistivity and causes phase shift only in a small area. The induced heating in the passive shield is 4% of the heating in the workpiece, which is lower than the power dissipation in the steel shield, but the deterioration of the heating process is worse with the copper shield. The magnetic steel shield also captures the field lines from the active compensation coils, so that a high compensation current outside the shield hardly influences the heating process.

E. Globally Optimized Passive and Active Shield

For the global optimization of active and passive shield, the same GA is used as above, but as the number of variables is now 13—the same 11 coil positions plus the position and height of the passive shield—the number of subpopulations is increased to six and the total number of individuals is 180. There are boundary limits on the extra two variables: the horizontal position of the passive shield is between 0.23 and 0.45 m, and its vertical length is in the range 0.04–0.30 m. An extra constraint forces the lowest compensation coil (coil 9) to be outside the passive shield. As a function evaluation takes more time, the total CPU time was 14 days.

Numerical experiments show that when heavily penalizing the compensation current and the heating in the passive shield—w_2 and w_3 in the expression of the objective value (1)—the optimized steel sheet corresponds to a higher average norm of B in the target area than with a fixed passive shield (2.99 μT versus 1.59 μT in Table III). The optimal cost of the objective function was 5000, consisting of four penalization terms: 2990 for the average field (w_1), 266 for the active shield dissipation (w_2), 954 for the passive shield dissipation (w_3), and 790 for the disturbance of the heating process (w_4). The GA has chosen the passive shield further from the excitation coil (at 0.325 m radius, 0.150 m high), so that the heating in it is only 191 W instead of 211 W. Also, the current is chosen 7.5 times lower than in the optimization with fixed passive shield (Table IV). The consequence is the same as in Section VII-C: the ten turns in coil 9 are not sufficient to reduce the field in the lower left corner of the target area, because the current in this coil together with the current in the passive shield are not high enough. With a high shield close to the excitation coil, an average field of 0.99 μT is possible, but this solution was rejected by the GA because the dissipation in the shield was then 1.2 kW.

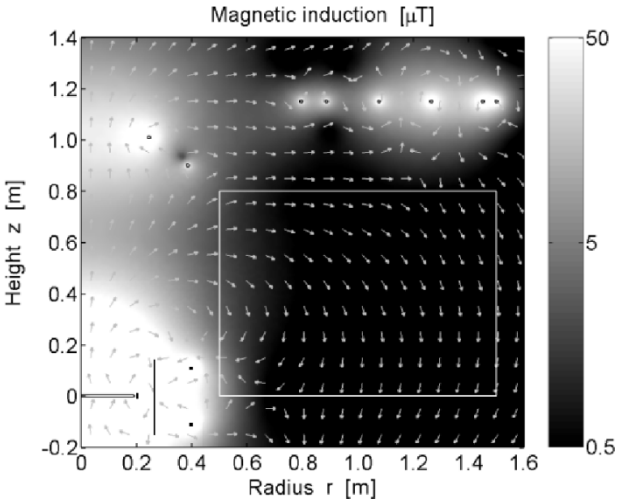

Fig. 11. Magnetic induction in μT in case of globally optimized passive (copper) and active shield.

For the optimization with the copper shield, w_2, w_3, and w_4 were chosen rather low. Consequently, the average field with nine independent currents was extremely low: 0.412 μT—almost 37 dB reduction. With all coils in series, the average value increased to 0.532 μT with 2×36 turns and only 0.18–1.43i A current (Table III, Table IV, and Fig. 11). The low values for the average field and the compensation current are partially due to the passive shield, which is quite high (0.145 m) and quite close to the excitation coil ($r = 0.264$ m). By consequence, the decrease in the heating power equals 17% and the heating in the passive shield is 169 W. These disadvantageous effects were penalized by almost doubling the cost, although the corresponding weighting factors were not really high. This shield was chosen because of the impressive field reduction in the target area. If the disturbance of the heating process or the dissipation in the passive shield are unacceptable, w_3 and w_4 in (1) should be chosen higher, depending on the demands for the design of the induction heater shield. Notice that the impact of the weighting factors depends on the shield material. For example: $w_3 = 5$ in Table III for the global optimization with the steel shield and for the global optimization with the copper shield. The dissipation in the steel shield is much larger than in the copper shield. This means that this choice of w_3 causes a strong impact on the objective function for the optimization with the steel shield, while it has only a moderate effect in the optimization with the copper shield.

Although simulation results are shown only for one frequency and one geometry, the optimization algorithm returns similar results for other geometries and frequencies.

VIII. Experimental Evaluation of the Numerical Model

To evaluate the numerical model, simulation results were compared with measurements on an experimental setup. This simulation has the same geometry of the induction heater with the steel passive shield as the other simulations in this paper (Table II). All compensation coil positions were chosen fixed as in Table V, corresponding the experimental setup. The geometry

TABLE V
Fixed Compensation Coil Positions, Optimal Compensation Current, and Number of Coil Turns Used in a Simulation to Compare Simulation Results With Experimentally Determined Results. Excitation Current is 40 A at 1 kHz

Shield	**Steel, fix**		
I_{opt}	$0.0371 - 0.0379i$ A		
Coil	r_i [m]	z_i [m]	t_i
1	0.300	0.600	8
2	0.400	0.900	4
3	0.500	1.150	−4
4	0.700	1.150	6
5	0.900	1.150	−4
6	1.100	1.150	4
7	1.300	1.150	−3
8	1.500	1.150	2
9	0.365	0.080	−1

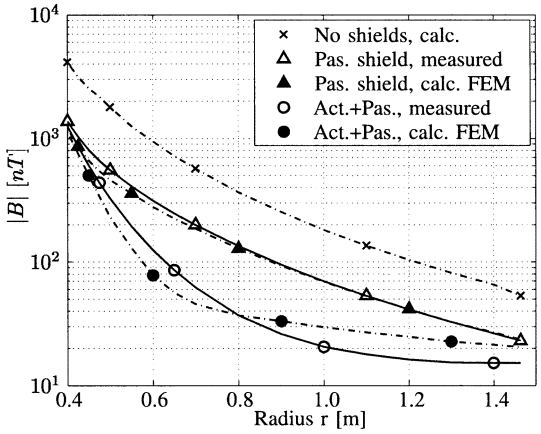

Fig. 12. Comparison of simulation and experimental results in the $z = 0$ plane at 1 kHz.

of the induction heater in the experimental setup also has the same geometry of excitation coil and workpiece as mentioned in Table II and in the FE layout of Fig. 4. The optimized active shield consists of 2×9 compensation coils—nine coils above the symmetry plane $z = 0$ and nine below the plane—with positions and number of turns shown in Table V. The coils have about 18 Ω resistance and 14 mH inductance ($18 + 9i\ \Omega$ impedance at 1 kHz). The test setup of the shielded induction heater is at real scale: the total height of the shielded induction heater is 2.3 m and the diameter is 3 m. Due to the laboratory limitations for the excitation current, a sinusoidal excitation current reduced to 40 A at 1 kHz instead of 4 kA is used both in the simulation and in the experiment. In the experimental setup, the PC-based data acquisition system samples the current in the excitation coil at 100 samples per period and calculates the required compensation current in the active shield. The latter is generated by a linear amplifier of 100 VA. The magnetic induction is measured by a 3-D probe with sensitivity 1 V/10 μT and frequency range 50 Hz–100 kHz. The probe is a 3-D version of the loop antenna in [12], but with small coils of 40-mm diameter instead of 250 mm. To avoid disturbance of the measurements by ambient fields (mainly 50 Hz), 1000 excitation periods are measured and a Fourier analysis is executed.

Fig. 12 compares the measurements on the induction heater test setup with the numerical results in the $z = 0$ plane. The

correspondence between the curves obtained with only a passive shield present (no active shield) is good: the average relative error to the measurement compared to the simulation is 8% (standard deviation $\sigma_d = 66$ nT). With passive and active shield, this relative error is 31% ($\sigma_d = 51$ nT), but the induction levels are low in the target area. As the absolute error is small, we can conclude that the numerical model shows sufficient correlation with the measurements.

IX. Conclusion

To reduce the magnetic stray field of induction heaters, a strategy for designing passive and active shields is discussed. To comply with the reference levels indicated by the international standards, the stray fields usually produced by induction heating equipment should be reduced up to ten times (20 dB). First, a numerical model of the induction heater with passive and active shields was developed. This numerical simulation takes into account some practical aspects related to the position of the passive and active shields and the currents in the compensation coils. Second, this numerical model was combined with a least-squares routine and a GA to find the best compensation currents and the best number of turns. Finally, a main GA calculates the best coil positions. The global optimization of active and passive shield gives the most flexibility with respect to limitations on compensation current, dissipation in passive shield, and influence on the heating process. This mode requires a lot of CPU time, but allows to achieve very low field levels if the mentioned limitations are not too restrictive: for this geometry, the discussed active and passive shield combinations are all able to reduce the average magnetic induction in the target area by more than 25 dB.

References

[1] B. Floderus, C. Stenlund, and F. Carlgren, "Occupational exposures to high frequency electromagnetic fields in the indermediate range ($>$ 300Hz–10 MHz)," *Bioelectromagnetics*, vol. 23, pp. 568–577, 2002.

[2] ICNIRP ICNIRP-Guidelines, "Guidelines for limiting exposure to time-varying electric, magnetic, and electromagnetic fields (up to 300 GHz)," *Health Phys.*, vol. 74, pp. 494–522, Apr. 1998.

[3] R. B. Schulz, V. C. Plantz, and D. R. Brush, "Shielding theory and practice," *IEEE Trans. Electromagn. Compat.*, vol. 30, pp. 187–201, Aug. 1988.

[4] P. Girdinio and M. Nervi, "Techniques for the automatic optimization of active shields," *COMPEL*, vol. 20, pp. 732–739, 2001.

[5] P. E. Gill, W. Murray, and M. H. Wright, *Practical Optimization*. London, U.K.: Academic, 1981.

[6] P. Sergeant, L. Dupré, J. Melkebeek, and L. Vandenbossche, "Magnetic field computation for optimized shielding of induction heaters," *J. Comp. Appl. Math.*, to be published.

[7] D. B. Fogel, "An introduction to simulated evolutionary optimization," *IEEE Trans. Neural Networks*, vol. 5, pp. 3–14, Jan. 1994.

[8] J. E. Baker, "Reducing bias and inefficiency in the selection algorithm," in *Proc. 2nd Int. Conf. Genetic Algorithms and Their Application*, Hillsdale, NJ, Oct. 1987, pp. 14–21.

[9] G. Syswerda, "Uniform crossover in genetic algorithms," in *Proc. 3rd Int. Conf. Genetic Algorithms*, San Mateo, CA, Dec. 1989, pp. 2–9.

[10] H. Mühlenbein and D. Schlierkamp-Voosen, "Predictive models for the breeder genetic algorithm: I. Continuous parameter optimization," *Evol. Comput.*, vol. 1, pp. 25–49, 1993.

[11] P. P. Silvester and R. L. Ferrari, *Finite Elements for Electrical Engineers*. Cambridge, U.K.: Cambridge Univ. Press, 1990.

[12] P. Sergeant and A. Van den Bossche, "High sensitivity 50 Hz–1 MHz probe for B and dB/dt," in *IEEE Int. Conf. Electromagn. Comp.*, Minneapolis, MN, Aug. 2002, pp. 55–60.

Peter L. Sergeant was born in 1978. He received the electrical and mechanical engineering degree from Ghent University, Ghent, Belgium, in 2001.

He joined the Department of Electrical Energy, Systems and Automation, Ghent University, in 2001 as a Research Assistant. His main research interests are numerical methods in electromagnetics, measurement techniques, and magnetic shielding.

Luc R. Dupré (M'01) was born in 1966. He received the electrical and mechanical engineering degree in 1989 and the Doctor in Applied Sciences degree in 1995, both from Ghent University, Ghent, Belgium.

He joined the Department of Electrical Energy, Systems and Automation, Ghent University, in 1989 as a Research Assistant. From 1996 until 2003, he was a Post-Doctoral Researcher for the Fund of Scientific Research-Flanders (FWO). Since 2003, he has been a Research Professor at Ghent University. His research interests mainly concern numerical methods for electromagnetics, especially in electrical machines, modeling, and characterization of magnetic materials.

Marc De Wulf was born in 1971. He received the electrotechnical engineering degree in 1995 and the Doctor in Applied Sciences degree in 2002 from Ghent University, Ghent, Belgium.

He joined the Department of Electrical Energy, Systems and Automation, Ghent University, in 1996 as a Research Assistant. Since 2002, he has been a Post-Doctoral Researcher at the Laboratory for Electrical Energy. His research interests include the characterization and modeling of magnetic materials, instrumentation and measurement techniques, and power electronics.

Jan A. A. Melkebeek (M'82–SM'84) was born in 1952. He received the electrical and mechanical engineering degree in 1975, the Doctor in Applied Sciences degree in 1980, and the "Doctor Habilitus" in electrical and electronical power technology in 1986, all from the Ghent University, Ghent, Belgium.

He was a visiting Professor at the Université Nazionale de Rwanda in Bultare, Rwanda, Africa, in 1981 and a visiting Assistant Professor at the University of Wisconsin, Madison, in 1982. Since 1987, he has been a Professor in electrical engineering at the Engineering Faculty of the Ghent University. Since 1993, he has also been the Head of the Department of Electrical Power Engineering. His teaching activities and research interests include electrical machines, power electronics, variable frequency drives, and control systems theory applied to electrical drives.